The Journal of Chemical Physics

# A nonequilibrium thermodynamics perspective of thixotropy

Cite as: J. Chem. Phys. **149**, 244902 (2018); https://doi.org/10.1063/1.5049397
Submitted: 21 July 2018 . Accepted: 30 November 2018 . Published Online: 26 December 2018

Pavlos S. Stephanou, and Georgios G. Georgiou

# A nonequilibrium thermodynamics perspective of thixotropy

Pavlos S. Stephanou[1,2,a)] and Georgios G. Georgiou[1]
[1]*Department of Mathematics and Statistics, University of Cyprus, P.O. Box 20537, 1678 Nicosia, Cyprus*
[2]*Department of Chemical Engineering, University of Patras, Patras GR26504, Greece*

(Received 21 July 2018; accepted 30 November 2018; published online 26 December 2018)

We propose a new description of elasto-viscoplastic fluids by relating the notion of thixotropy directly to internal viscoelasticity and network structures through a general, thermodynamically consistent approach. By means of non-equilibrium thermodynamics, a thermodynamically admissible elasto-viscoplastic model is derived which introduces self-consistently and effortlessly thixotropic effects and reproduces at both low and high shear rates experimental data usually fitted with empirical constitutive equations, such as the Bingham and Herschel-Bulkley models. The predictions of the new model are in very good agreement with available steady-state shear rheological data for soft colloidal pastes and blood, i.e., systems exhibiting a yield stress, and with time-dependent rheological data for blood, i.e., during a triangular time-dependent change in the shear rate, exhibiting a hysteresis. The proposed approach is expected to provide the means to improve our understanding of thixotropic fluids. *Published by AIP Publishing.* https://doi.org/10.1063/1.5049397

## I. INTRODUCTION

Many materials of industrial interest, such as emulsions, colloids, suspensions, and foams, exhibit a yield stress, i.e., they flow only above this critical stress and behave as elastic solids otherwise.[1,2] Such materials are encountered in many sectors, such as in the oil industry (e.g., crude oil and drilling fluids), the construction sector (e.g., cement pastes and fresh concrete), the food industry (e.g., ketchup, margarine, and mayonnaise), and the pharmaceutics/cosmetics industry (e.g., blood, pastes, and foams).[1,2] The yield stress is acknowledged as an "engineering" reality and has been the subject of ongoing debate.[3] The description of yield-stress materials has been proven to be one of the subtlest tasks in rheology.[4] However, a more in-depth understanding of their peculiar rheological behaviour is paramount if we aspire to optimize the processing properties of this important class of materials.

The appearance of a yield stress is a rheological feature strongly associated with thixotropic fluids.[5] According to the International Union of Pure and Applied Chemists (IUPAC), thixotropy is defined as the continuous decrease of viscosity with time when flow is applied to a sample that has been previously at rest and the subsequent recovery of viscosity in time when the flow is discontinued.[5,6] However, such a behaviour is also encountered with viscoelastic, shear-thinning, fluids: upon a stepwise increase in the shear rate, the viscosity, after an initial overshoot, decreases, whereas when a stepwise reduction is applied, the viscosity gradually returns to a higher value. Clearly, distinguishing between thixotropy and nonlinear viscoelasticity is important in our understanding of these phenomena.[7] Another characteristic rheological feature of thixotropic fluids is the hysteresis experiment where the shear rate, $\dot{\gamma}$, is first gradually increased with time $\dot{\gamma} = \alpha t$, $0 < t < t_{\rm m}$ and then decreased following $\dot{\gamma} = \alpha(2t_{\rm m} - t)$, $t_{\rm m} < t < 2t_{\rm m}$, with $\alpha = \dot{\gamma}_{\rm max}/t_m$, where $\dot{\gamma}_{\rm max}$ is the maximum shear rate reached (at $t = t_{\rm m}$).[5] When the transient shear stress is plotted as a function of the time-dependent shear rate, a hysteresis loop is observed in thixotropic fluids (see, e.g., Fig. 2 of Ref. 5 and Figs. 3 and 7).

The simplest model available for the description of yield-stress fluids, also known as viscoplastic fluids, is the Bingham model, which involves two material parameters (the yield stress, $\sigma_y$, and the plastic viscosity, $\eta_B$)[1,8]

$$\begin{cases} \dot{\boldsymbol{\gamma}} = \mathbf{0}, & \sigma \le \sigma_y \\ \boldsymbol{\sigma} = \left(\dfrac{\sigma_y}{\dot{\gamma}} + \eta_{\rm B}\right)\dot{\boldsymbol{\gamma}}, & \sigma > \sigma_y, \end{cases} \tag{1}$$

where $\boldsymbol{\sigma}$ is the extra (polymeric) stress tensor, $\dot{\boldsymbol{\gamma}} \equiv \nabla\mathbf{u} + (\nabla\mathbf{u})^T$ is the rate-of-strain tensor, and $\sigma \equiv \sqrt{\frac{1}{2}\boldsymbol{\sigma} : \boldsymbol{\sigma}}$ and $\dot{\gamma} \equiv \sqrt{\frac{1}{2}\dot{\boldsymbol{\gamma}} : \dot{\boldsymbol{\gamma}}}$ denote the magnitudes of the two tensors (the latter denotes the shear rate). In shear flow, the shear stress approaches the yield stress at small shear rates and behaves as a Newtonian fluid at large shear rates. An extension of this model is the Herschel-Bulkley (HB) model given as

$$\begin{cases} \dot{\boldsymbol{\gamma}} = \mathbf{0}, & \sigma \le \sigma_y \\ \boldsymbol{\sigma} = \left(\dfrac{\sigma_y}{\dot{\gamma}} + K\dot{\gamma}^{n-1}\right)\dot{\boldsymbol{\gamma}}, & \sigma > \sigma_y, \end{cases} \tag{2}$$

where $K$ is the consistency index and $n$ is the flow behaviour index (power-law exponent);[1,8] the Bingham model is a special case of the HB model when $n = 1$ and $K = \eta_B$. The HB model is able to describe a shear thinning ($n < 1$) or shear thickening ($n > 1$) behaviour. Both the Bingham and HB models, which are routinely employed to describe the behavior of various viscoplastic materials, belong to the class of generalized

a)Author to whom correspondence should be addressed: stefanou.pavlos@ucy.ac.cy

Newtonian constitutive equations, i.e., they do not account for viscoelastic effects.[1] It should also be emphasized that, despite their success, when fitting data using these models, the material parameters involved are phenomenological in nature and bear no physical meaning, i.e., they cannot be related to the molecular characteristics of the particular material they aim to describe. Furthermore, they exhibit an unavoidable disadvantage: they predict vanishing normal stresses in shear flow.[5,9]

The complex rheological behavior of thixotropic fluids, in general, can be understood on the basis of a microstructure that depends on the shear history.[5] For example, Carbopol solutions are made of high-molecular-weight structural elements that interact forming complex network-like structures.[10] The continued competition between the flow-induced breakdown and the thermal-noise-induced buildup of the structural elements characterizes their rheological behaviour. Under extreme flow conditions, the breakdown of the structure prevails recombination, leading to a complete destruction of the elastic network. Another example is suspensions, e.g., drilling fluids, for which the existence of a yield stress is attributed to the combined effect of the solid network of connected particles and the dry friction between loose particles;[11] the destruction of the network is the result of viscous forces acting on the particles due to flow. Finally, in the case of crude oil, the elastic network is believed to be the result of crystalline formations composed of paraffine, asphaltane, and resin constituents.[9]

From a mathematical point of view, the internal structure may be characterized by a scalar structural variable, $\lambda$, that expresses the instantaneous degree of structure: in a fully structured state, i.e., a complete network that deforms elastically, it is equal to unity, while in a completely broken state it vanishes.[5] Thus, the equation for the shear stress is coupled with $\lambda$, e.g., in the case of the HB model $\sigma_{yx}(\lambda) = \sigma_y(\lambda) + K_{HB}(\lambda)\dot{\gamma}^{n(\lambda)}$.[5,9,11] The rate of change in the $\lambda$ is the net result of the simultaneous rates for structure buildup and breakdown which follow certain kinetics.[5] One of the earliest thixotropic constitutive models of this class is that proposed by Moore[12] in which the stress tensor is given as $\boldsymbol{\sigma} = \eta(\lambda)\dot{\boldsymbol{\gamma}}$ where $\lambda$ is dictated by $\partial_t\lambda = k_2(1-\lambda) - k_1\lambda$, where $k_2$ and $k_1$ are the rates of buildup and destruction, respectively, which could depend on (the invariants of) $\dot{\boldsymbol{\gamma}}$ and on $\lambda$. Another early model is that of Fredrickson[13] wherein the stress tensor is given as $\boldsymbol{\sigma} = \phi^{-1}\dot{\boldsymbol{\gamma}}$ and the structural parameter, characterized as "fluidity" $\phi$, obeys $\partial_t\phi = k_2(\phi_0 - \phi) - k_1(\phi_\infty - \phi)\boldsymbol{\sigma} : \dot{\boldsymbol{\gamma}}$; thus, it can be deduced that $\lambda = (\phi - \phi_0)/(\phi_\infty - \phi_0)$. Many more viscoplastic constitutive models have been proposed in the literature.[5]

However, common viscoplastic constitutive models still ignore elastic effects once the fluids start flowing. This omission has led to the development of elasto-viscoplastic constitutive models describing the rheological behavior of the fluid above the yield stress via the use of viscoelastic models, such as the Oldroyd-B,[14] the Maxwell,[15] or the Phan-Thien Tanner[16] models. Even though some of these models have proven to describe well the experimental data,[12] their connection with molecular structures is vague. Furthermore, the mere hybridization of viscoplasticity and elasticity may not be done appropriately, possibly lacking self-consistency. These drawbacks are detrimental in the potential use of elasto-viscoplastic models to enhance our understanding of the rheological behavior of thixotropic fluids.

To remedy the above shortcomings, we herein propose a detailed model for thixotropic materials that can be related to their molecular underpinning and provide a self-consistent coupling between elasticity and viscoplasticity through the consideration of an elastic free energy expression [see Eqs. (5)]. The generalized-bracket[17] formalism of non-equilibrium thermodynamics (NET) is employed to properly address three key issues: (a) selecting the proper state variables, (b) constructing both the Poisson and dissipation brackets, and (c) specifying the system's Hamiltonian. The attractive advantage of employing a NET formalism[17–19] is that the resulting constitutive model is, by construction, consistent with the laws of thermodynamics.[17–19] NET laws provide the means to impose restrictions to the model parameters. Up to date, several micro-structured systems, such as liquid crystals,[20–22] polymer melts and solutions,[17–19,23,24] immiscible complex fluids,[17–19,26–28] polymer nanocomposites,[29–34] drilling fluids,[35] blood,[36] and ionomers,[37] have been addressed through NET, a fact that attests to its usefulness and applicability. To the best of our knowledge, only the model proposed by Beris *et al.*[38] for concentrated star polymer suspensions, a system exhibiting a yield stress, was derived via the use of NET principles. This model is based on an extension of the Johnson–Segalman viscoelastic constitutive equation in which the non-affine parameter is variable, obeying an evolution equation that is purely phenomenological and not derived from NET. Beris *et al.*[38] also proposed phenomenological elastic and viscous contributions to the shear stress, not derived from NET.

## II. NONEQUILIBRIUM THERMODYNAMICS MODELING OF THIXOTROPY

### A. The vector of state variables

Following a previous study,[5] we choose to employ a scalar structural variable, $\lambda$, to characterize the instantaneous degree of the structure of thixotropic materials by accounting for the number of segments or components that are attached to the underlying network. We also employ an additional tensorial structural variable, $\mathbf{C}$, to characterize the deformation of the complex structure, where each segment is modeled as an elastic dumbbell that can be detached from the network due to flow and attached to it due to thermal noise. The use of NET allows for the proper coupling of these two structural variables with the hydrodynamic ones and with each other. Herein, we consider a homogeneous, isothermal, and incompressible flow. The number density, $n$, and the mass density of polymer segments, $\rho$, are related through $n = (\rho/M)N_{Av}$, where $M$ denotes the segment molecular weight of each chain (i.e., a strictly monodisperse system is considered) and $N_{\text{av}}$ is Avogadro's constant. The conformation tensor density is defined by $\mathbf{C} = \rho\mathbf{c}$, where $\mathbf{c} = \int \mathbf{RR}\psi(\mathbf{R}, t)d^3\mathbf{R}$ is the second moment of the distribution function $\psi(\mathbf{R}, t)$ for the end-to-end connector vector $\mathbf{R}$.[17–19,23] Note that as the mass density of polymer segments is constant, due to incompressibility, the

conformation tensor $\mathbf{c}$ may be employed directly.[17] Finally, we consider the momentum density $\mathbf{m}$ as the hydrodynamic variable. Overall, the vector $\mathbf{x}$ of state variables is expressed as $\mathbf{x} = \{\mathbf{m}, \lambda, \mathbf{c}\}$. Since the system is isothermal, the entropy density (or temperature) is excluded from the vector of state variables.

### B. The Hamiltonian of the system

In the present case, the mechanical part of the system's Hamiltonian is given by

$$H_m = K_{en}(\mathbf{x}) + A(\mathbf{x}), \tag{3}$$

where

$$K_{en}(\mathbf{x}) = \int \frac{\mathbf{M}^2}{2\rho} dV. \tag{4}$$

The first term on the right-hand side of Eq. (3) represents the kinetic energy of the system, $K_{en}(\mathbf{x})$, given via Eq. (4), whereas $A(\mathbf{x})$ represents the system's Helmholtz free energy, given by

$$\begin{aligned} A(\mathbf{x}) &= \int a(\mathbf{x}) dV = \int [a_{el}(\mathbf{x}) + a_{mix}(\mathbf{x})] dV, \\ &\frac{G}{2}\int \left[\frac{K}{k_B T} tr\left(\mathbf{c} - \mathbf{c}_{eq}\right) - \ln\det\tilde{\mathbf{c}}\right] dV + \frac{G}{2}\int (\lambda \ln\lambda - \lambda + 1) dV, \end{aligned} \tag{5}$$

where $G = nk_BT = \rho RT/M$ is the (constant) elastic modulus, $K$ is the dumbbell's spring constant, $\tilde{\mathbf{c}} = (K/k_BT)\mathbf{c}$ is the dimensionless conformation tensor, $k_B$ is Boltzmann's constant, and $T$ is the absolute temperature. It should be noted that in the present approach the polymeric segments are assumed to be below the entanglement threshold; however, there are available free energy expressions that can be used beyond this threshold.[18,19,24] The first integral in Eq. (5) expresses the sum of the elastic energy of the Hookean springs, wherein all segments are deformed due to the imposed flow. The second integral expresses the ideal entropy of mixing for segments that are not associated with the network; the extra term is added to ensure that the mixing free energy maximizes under no flow conditions, i.e., when $\lambda = 1$ (see further discussion below).

### C. The Poisson and dissipation brackets

For a system for which its internal structure is described by a conformation tensor, the expression for the Poisson bracket is well known (see, e.g., Refs. 17–19)

$$\begin{aligned} \{F, G\} = &-\int \left[\frac{\delta F}{\delta m_\gamma}\nabla_\beta\left(m_\gamma \frac{\delta G}{\delta m_\beta}\right) - \frac{\delta G}{\delta m_\gamma}\nabla_\beta\left(m_\gamma \frac{\delta F}{\delta m_\beta}\right)\right] dV \\ &-\int \left[\frac{\delta F}{\delta c_{\alpha\beta}}\nabla_\gamma\left(c_{\alpha\beta}\frac{\delta G}{\delta m_\gamma}\right) - \frac{\delta G}{\delta c_{\alpha\beta}}\nabla_\gamma\left(c_{\alpha\beta}\frac{\delta F}{\delta m_\gamma}\right)\right] dV \\ &+\int c_{\gamma\alpha}\left[\frac{\delta F}{\delta c_{\alpha\beta}}\nabla_\gamma\left(\frac{\delta G}{\delta m_\beta}\right) - \frac{\delta G}{\delta c_{\alpha\beta}}\nabla_\gamma\left(\frac{\delta F}{\delta m_\beta}\right)\right] dV \\ &+\int c_{\gamma\beta}\left[\frac{\delta F}{\delta c_{\alpha\beta}}\nabla_\gamma\left(\frac{\delta G}{\delta m_\alpha}\right) - \frac{\delta G}{\delta c_{\alpha\beta}}\nabla_\gamma\left(\frac{\delta F}{\delta m_\alpha}\right)\right] dV \\ &+\int g_{\gamma\alpha}\left[\frac{\delta F}{\delta \lambda}\nabla_\gamma\left(\frac{\delta G}{\delta m_\alpha}\right) - \frac{\delta G}{\delta \lambda}\nabla_\gamma\left(\frac{\delta F}{\delta m_\alpha}\right)\right] dV. \end{aligned} \tag{6}$$

Note that here, and throughout this work, Einstein's summation convention for repeated Greek indices is employed. The first four integrals represent the usual Poisson bracket for the isothermal and incompressible flow of a viscoelastic fluid whose structure is characterized by a conformation tensor.[17–19,23] The last integral in Eq. (6) introduces a general coupling between the scalar structural variable and the velocity gradient through the tensor $\mathbf{g}$.[19] Since we need to impose the requirement that the Poisson bracket fulfils the Jacobi identity, the following restrictions are obtained when the most general expression for $\mathbf{g}$ is considered, $\mathbf{g} = g_1\tilde{\mathbf{c}} + g_2\boldsymbol{\delta} + g_3\tilde{\mathbf{c}}^{-1}$ according to the Cayley-Hamilton theorem [where the scalar coefficients are functions of $\lambda$ and the three invariants of the dimensionless conformation tensor: $I_1 = tr\tilde{\mathbf{c}}, I_2 = \ln\det\tilde{\mathbf{c}}$, $I_3 = -tr\tilde{\mathbf{c}}^{-1}$]:[19]

$$\begin{aligned} g_1\frac{\partial g_2}{\partial\lambda} - g_2\frac{\partial g_1}{\partial\lambda} &= 2\left(\frac{\partial g_1}{\partial I_2} - \frac{\partial g_2}{\partial I_1}\right), \\ g_1\frac{\partial g_3}{\partial\lambda} - g_3\frac{\partial g_1}{\partial\lambda} &= 2\left(\frac{\partial g_1}{\partial I_3} - \frac{\partial g_3}{\partial I_1}\right), \\ g_2\frac{\partial g_3}{\partial\lambda} - g_3\frac{\partial g_2}{\partial\lambda} &= 2\left(\frac{\partial g_2}{\partial I_3} - \frac{\partial g_3}{\partial I_2}\right). \end{aligned} \tag{7}$$

The corresponding dissipation bracket used in this work is of the following form:

$$\begin{aligned} [F, G]_{nec} = &-\int \frac{\delta F}{\delta c_{\alpha\beta}}\Lambda^c_{\alpha\beta\gamma\varepsilon}\frac{\delta G}{\delta c_{\gamma\varepsilon}} dV - \int \frac{\delta F}{\delta\lambda}\Lambda^\lambda\frac{\delta G}{\delta\lambda} dV \\ &-\int \nabla_\alpha\left(\frac{\delta F}{\delta M_\beta}\right) Q_{\alpha\beta\gamma\varepsilon}\nabla_\gamma\left(\frac{\delta G}{\delta M_\varepsilon}\right) dV. \end{aligned} \tag{8}$$

The first two integrals on the right-hand side of Eq. (8) account for relaxation effects for both structural variables and are proportional to a fourth-rank relaxation tensor, $\Lambda^c_{\alpha\beta\gamma\varepsilon}$, and a scalar relaxation factor $\Lambda^\lambda$, which, in turn, are inversely proportional to some characteristic relaxation times. The third integral accounts for the viscous dissipation of the solvent and expresses the Newtonian rheological behavior of the solvent; it is proportional to the fourth-rank tensor $Q_{\alpha\beta\gamma\varepsilon}$. Note that the subscript "nec," meaning "no entropy production correction," is added to the dissipation bracket to indicate that this dissipation bracket is without terms involving Volterra derivatives with respect to entropy,[17] which are not important when considering (as we do here) isothermal systems.

### D. The resulting evolution equations

Following the usual procedure,[17] the following expressions are obtained for the Cauchy momentum balance equation, the evolution equations for the conformation tensor $\mathbf{c}$ and the scalar structural variable $\lambda$, and the extra stress tensor:

$$\rho\frac{\partial\mathbf{v}}{\partial t} = -\rho\mathbf{v}\cdot\nabla\mathbf{v} - \nabla\cdot P + \nabla\cdot\boldsymbol{\sigma}, \tag{9a}$$

$$\dot{c}_{\alpha\beta,[1]} = -\Lambda^c_{\alpha\beta\gamma\varepsilon}\frac{\delta A}{\delta c_{\gamma\varepsilon}}, \tag{9b}$$

$$\frac{D\lambda}{Dt} = -\Lambda^\lambda\frac{\delta A}{\delta\lambda} + \boldsymbol{\kappa} : \mathbf{g}, \tag{9c}$$

$$\sigma_{\alpha\beta} = 2c_{\alpha\gamma}\frac{\delta A}{\delta c_{\gamma\beta}} + g_{\alpha\beta}\frac{\delta A}{\delta\lambda}. \tag{9d}$$

The following typical expressions, proposed in the literature for viscoelastic fluids,[17] are also used:

$$\Lambda^{c}_{\alpha\beta\gamma\varepsilon} = \frac{1}{2nK\tau_R(tr\mathbf{c},\lambda)} \times \left(c_{\alpha\gamma}\delta_{\beta\varepsilon} + c_{\alpha\varepsilon}\delta_{\beta\gamma} + c_{\beta\gamma}\delta_{\alpha\varepsilon} + c_{\beta\varepsilon}\delta_{\alpha\gamma}\right), \tag{10a}$$

$$\Lambda^{\lambda} = \frac{2}{G\tau_\lambda}, \tag{10b}$$

$$Q_{\alpha\beta\gamma\varepsilon} = \eta_s\left(\delta_{\alpha\gamma}\delta_{\beta\varepsilon} + \delta_{\alpha\varepsilon}\delta_{\beta\gamma}\right), \tag{10c}$$

where $\eta_s$ is the (constant) solvent viscosity, $\tau_R$ is the characteristic relaxation time of segments (usually of macromolecular nature) in their non-associative state, and $\tau_\lambda$ is a characteristic time for the scalar structural variable. Furthermore, in what follows, we consider $\mathbf{g} = -\tilde{\mathbf{c}}\lambda$ that duly satisfies restrictions Eqs. (7).

Finally, the following time evolution equations are derived for the scalar structural variable and the dimensionless conformation tensor, and the expression for the extra stress tensor:

$$\begin{aligned}\overset{\cdot}{\mathbf{c}}_{[1]} &\equiv \frac{\partial \mathbf{c}}{\partial t} + \mathbf{v}\cdot\nabla\mathbf{c} - (\nabla\mathbf{v})^T\cdot\mathbf{c} - \mathbf{c}\cdot\nabla\mathbf{v} \\ &= -\frac{1}{\tau_R(tr\tilde{\mathbf{c}}\lambda)}\left(\mathbf{c} - \frac{k_BT}{K}\boldsymbol{\delta}\right),\end{aligned} \tag{11}$$

$$\frac{D\lambda}{Dt} = -\frac{1}{\tau_\lambda}\ln\lambda - (\boldsymbol{\kappa}:\tilde{\mathbf{c}})\lambda, \tag{12}$$

$$\begin{aligned}\boldsymbol{\sigma} &= G(\tilde{\mathbf{c}} - \boldsymbol{\delta}) - \frac{G}{2}\lambda(\ln\lambda)\tilde{\mathbf{c}} + \eta_s\dot{\boldsymbol{\gamma}} \Rightarrow \\ \tilde{\boldsymbol{\sigma}} &= \tilde{\mathbf{c}} - \boldsymbol{\delta} - \left(\frac{1}{2}\lambda\ln\lambda\right)\tilde{\mathbf{c}} + \beta_s\tilde{\dot{\boldsymbol{\gamma}}}.\end{aligned} \tag{13}$$

The thermodynamic pressure $P$ is given by[17]

$$P = \mathbf{c}:\frac{\delta A}{\delta \mathbf{c}} - a(\mathbf{x}), \tag{14}$$

where $\tilde{\boldsymbol{\sigma}} = \boldsymbol{\sigma}/G$, $\boldsymbol{\delta}$ is the unit tensor, and $\boldsymbol{\kappa} = (\nabla\mathbf{v})^T$. It should be pointed out that since the material of interest is incompressible, the pressure is no longer a thermodynamics state variable but some arbitrary scalar field that guarantees that the divergence-free condition automatically holds.[17] Equation (11) expresses the dynamics of the conformation tensor, where the definition of the upper-convected Maxwell time derivative is also provided. The segment's characteristic time is selected to be given by

$$\tau_R(tr\mathbf{c},\lambda) = \frac{\tau_{R,eq}}{1-\lambda}\left(\frac{\mathrm{tr}\mathbf{c}}{\mathrm{tr}\mathbf{c}_{eq}}\right)^k, \tag{15}$$

which is based on the extended White/Metzner (EWM) expression,[17,39] where $\tau_{R,eq}$ is the segment's characteristic time at equilibrium if the segments were not able to associate, and the exponent $k$ should be negative to account for a decreasing characteristic time due to flow (for shear-thinning fluids). The concentration dependency of $\tau_{R,eq}$ follows the theory of Zimm, according to which $\tau_{R,eq} \sim c^{(2-3\nu)/(3\nu-1)}$ where $c$ is the concentration and $\nu$ is the scaling exponent ($\nu = 1/2$ for theta-solvents and $\approx 0.588$ in good solvents).[40] Although other choices for the segment's characteristic time are, of course, possible, our above-stated choice will be shown below to capture the steady-state flow characteristics of the routinely employed HB model. Equation (12) describes the evolution equation for $\lambda$ involving a coupling between $\lambda$ and the velocity gradient in the second term, to account for the breakup of the network due to the imposed flow, and relaxation effects in the first term accounting for the buildup of the network; when making time (and the velocity gradient) dimensionless using $\tau_{R,eq}$, then a parameter $\varepsilon \equiv \tau_\lambda/\tau_{R,eq}$ appears in the denominator of the first term which expresses the ratio between the relaxation time associated with network buildup and the relaxation time of segments; thus, the parameter $\varepsilon$ quantifies the relative importance between two counteracting effects: regeneration/buildup and flow-induced breakup. This parameter is particularly important since, as will be shown below, it is intimately related to the existence of a yield stress in steady-state shear.

Equations (11)–(13) lie at the heart of this work. This approach leads unambiguously and self-consistently to the network buildup and destruction terms as described via Eq. (12). Thus, the necessity to resort to postulated and phenomenological expressions, as is routinely done in the literature,[5,9] is eliminated. Under no flow conditions, $\lambda = 1$ and the segment's relaxation time becomes infinite so that the conformation tensor evolution equation reads $\overset{\cdot}{\tilde{\mathbf{c}}}_{[1]} = 0$, bearing the solution $\tilde{\mathbf{c}} = \mathbf{B}(t,t')$, where $\mathbf{B}(t,t') = \mathbf{E}(t,t')\cdot\mathbf{E}^T(t,t')$ is the Finger strain tensor; this is the expected solution for the deformation of a solid network.[41]

## III. COMPARISONS WITH PREVIOUS WORK

It is important to see how the new rheological model as derived in the context of the generalized bracket formalism of NET compares with previous models.[5,9] In the case of shear flow close to equilibrium, Eq. (12) becomes $\partial_t\lambda = (1-\lambda)/\tau_\lambda - \dot{\gamma}\varepsilon^{-\frac{1}{2}}\lambda$ (since $\tilde{c}_{xy} \sim \varepsilon^{-1/2}$), which nicely matches previous models:[5] $\partial_t\lambda = k_2\dot{\gamma}^c(1-\lambda)^d - k_1\dot{\gamma}^a\lambda^b$ when $a = b = d = 1$, $c = 0$, $k_2 = 1/\tau_\lambda$, and $k_1 = \varepsilon^{-1/2}$. Of course, these exact expressions can be obtained within the formalism by choosing different expressions for $\mathbf{g}$ and the mixing free energy density. For example, when $\mathbf{g} = -k_1\dot{\gamma}^{a-2}\lambda^b\dot{\boldsymbol{\gamma}}$, one gets exactly the afore-mentioned destruction term; however, this selection does not couple the structural variable with the conformation tensor. In case we were to generalize $\mathbf{g}$ to include a more general tensorial function of the conformation tensor, we should take note of whether restrictions imposed by the Jacobi identity [Eqs. (7) ] are duly met. Similarly, when $a_{mix}(\mathbf{x}) = -G\frac{1}{d+1}(1-\lambda)^d$ and having the structural variable characteristic time decreasing due to the imposed flow as $\tau_\lambda \sim \dot{\gamma}^{-c}$ leads to the afore-mentioned regeneration term. A more appropriate form, however, irrespective of the choice of $a_{mix}$, could be identified by considering $\tau_\lambda = \tau_\lambda(\mathbf{c},\lambda)$.

Overall, and despite the fact that previous studies invoked phenomenological and empirical relations for the buildup and destruction of the network and how these are related to the deformation of the segments, it is obvious that they are similar to the proposed model; in fact, the buildup rate is herein generalized for beyond equilibrium cases, since it involves $\ln\lambda$. In

the present approach, the choice of the form of the destruction rate in Eq. (12) self-consistently specifies the extra stress tensor expression. This comes in complete contrast to previous studies, wherein the extra stress tensor is provided (introduced) externally. Ultimately, and given the similarity of the constitutive relations employed by previous approaches (at least close to equilibrium), the present model also stands as a verification of these approaches from a NET perspective, thus dictating their thermodynamic admissibility (see the Appendix).

## IV. ASYMPTOTIC BEHAVIOR IN STEADY STATE SHEAR AND UNIAXIAL ELONGATION

In this section, we proceed to analyze the asymptotic behavior of the model in the limit of low deformation rates for the following two types of flow: simple shear flow described by the kinematics $\mathbf{u} = (\dot{\gamma}y, 0, 0)$ and uniaxial elongation flow described by the kinematics $\mathbf{u} = \left(\dot{\varepsilon}x, -\frac{1}{2}\dot{\varepsilon}y, -\frac{1}{2}\dot{\varepsilon}z\right)$, where $\dot{\varepsilon}$ is the elongation rate. The material functions to analyze are the shear viscosity $\eta = \sigma_{yx}/\dot{\gamma}$ and the first normal stress coefficients $\Psi_1 = \left(\sigma_{xx} - \sigma_{yy}\right)/\dot{\gamma}^2$ in the case of shear (the second normal stress coefficient is identically zero), and the extensional viscosity $\eta_{\mathrm{E}} = \left(\sigma_{xx} - \sigma_{yy}\right)/\dot{\varepsilon}$ in the case of uniaxial elongation. To get asymptotic expressions for the conformation tensor and the structural variable, and consequently for the material functions under steady-state conditions, in shear and uniaxial elongation, we consider the limit of small deformation rates and linearize the algebraic equations. The following results are then obtained.

In shear flow, we have

$$\begin{aligned} &\lim_{\dot{\gamma}\to 0} \tilde{c}_{xx} = 1 + 2\varepsilon^{-1} \Rightarrow \lim_{\dot{\gamma}\to 0} \tilde{\sigma}_{xx} = 2\varepsilon^{-1}, \\ &\lim_{\dot{\gamma}\to 0} \tilde{c}_{xy} = \lim_{\dot{\gamma}\to 0} \tilde{\sigma}_{xy} \equiv \tilde{\sigma}_y = \varepsilon^{-1/2}, \\ &\lambda \approx 1 - \varepsilon^{1/2}\mathrm{Wi}, \end{aligned} \tag{16}$$

which imply that both the shear stress and the first normal stress difference approach a plateau in this limit, $\sigma_{xy} = G/\sqrt{\varepsilon}, N_1 \equiv \sigma_{xx} - \sigma_{yy} = 2G/\varepsilon$. The former expression is what is customarily referred to as the yield stress, $\sigma_y$, while the latter will be referred to as the yield first normal stress difference, $N_{1,y}$. It is easily observed that as the value of the parameter $\varepsilon$ increases, both $\sigma_y$ and $N_{1,y}$ decrease, and for $\varepsilon \gg 1$, neither a yield stress nor a yield first normal stress difference is predicted. In fact, $N_{1,y}$ dissipates much faster than $\sigma_y$. This is anticipated as when $\tau_\lambda \gg \tau_{R,eq}$ the buildup of the network takes much longer than its destruction and the network exhibits almost no resistance to flow.

In uniaxial elongation, we get

$$\begin{aligned} \lim_{\dot{\gamma}\to 0} \tilde{c}_{xx} &= 1 + \frac{1}{\varepsilon}\theta(\varepsilon), \\ \lim_{\dot{\gamma}\to 0} \tilde{c}_{yy} &= 2\frac{\varepsilon + \theta(\varepsilon)}{2\varepsilon + 3\theta(\varepsilon)}, \end{aligned} \tag{17a}$$

leading to

$$\begin{aligned} \lim_{\dot{\gamma}\to 0}\left(\tilde{\sigma}_{xx} - \tilde{\sigma}_{yy}\right) \equiv N_{\mathrm{E},y} &= \left[1 + \frac{1}{\varepsilon}\theta(\varepsilon)\right]\frac{3\theta(\varepsilon)}{2\varepsilon + 3\theta(\varepsilon)}, \\ \lambda &\approx 1 - 2\left(1 + \frac{\varepsilon}{\theta(\varepsilon)}\right)\mathrm{Wi}, \end{aligned} \tag{17b}$$

where

$$\theta(\varepsilon) = 1 + \sqrt{1 + \frac{4}{3}\varepsilon}. \tag{17c}$$

We thus note that a yielding behavior is also observed even in uniaxial elongation, where a yield elongation normal stress, $N_{\mathrm{E},y}$, is noted, although the expressions are more complicated functions of $\varepsilon$.

## V. PREDICTIONS OF THE NEW MODEL

### A. Shear flow

The predictions of the new model in the case of homogeneous simple shear for $\lambda$, shear stress, and first normal stress difference are plotted vs. the dimensionless shear rate, $\mathrm{Wi} = \dot{\gamma}\tau_{R,eq}$, for various values of $\varepsilon$ and $k$ in Fig. 1. We note

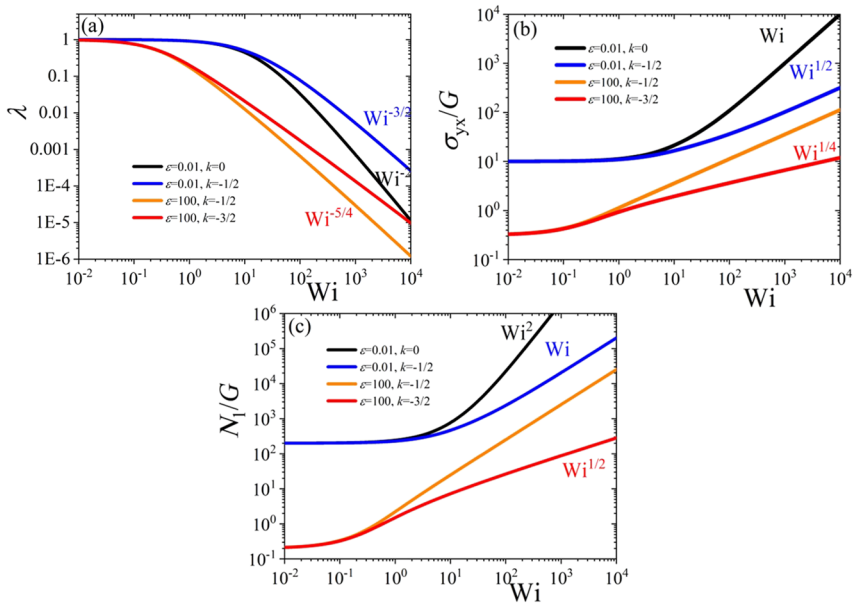


FIG. 1. Predictions of the new model for (a) $\lambda$, (b) shear stress, and (c) first normal stress difference as a function of dimensionless shear rate for selected values of the model parameters; a power-law behavior at large shear rates is observed.

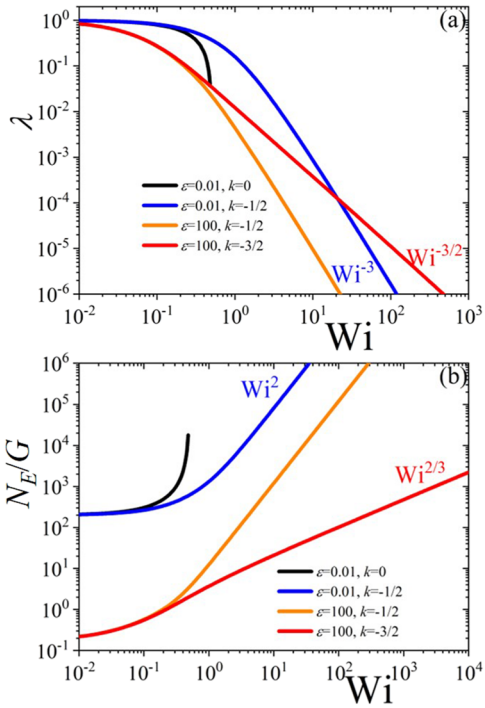


FIG. 2. Predictions of the new model for (a) $\lambda$ and (b) elongation stress as a function of dimensionless elongation rate for selected values of the model parameters; a power-law behavior at large elongation rates is noted.

that as $\mathrm{Wi} \ll 1$, both the shear stress and the first normal stress difference approach their yield values, $\sigma_y$ and $N_{1,y}$, respectively. As the dimensionless shear rate exceeds $\sim \varepsilon^{-1/2}$, the destruction of the network commences [Fig. 1(a)] leading to the increase in both the shear stress [Fig. 1(b)] and the first normal stress difference [Fig. 1(c)]. When segments deform with a constant relaxation time, i.e., $k = 0$, the shear stress, when $\mathrm{Wi} \gg 1$, increases linearly, while the first normal stress difference increases quadratically, with Wi. The former prediction, i.e., the exhibition of a constant viscosity at large shear rates, is reminiscent of the Bingham model. On the other hand, when $k \neq 0$, the shear stress power-law at large Wi is below the Bingham model predictions, which is reminiscent of the HB model, $\sigma_{yx} \sim \dot{\gamma}^n$; the exponent $n$ is related to $k$ via $n = (1 - 2k)^{-1}$. As an overall note, $\varepsilon$ controls the behavior close to equilibrium, and, therefore, the yielding behavior, whereas the exponent $k$ controls the behavior at large Wi. Note that would experimental data for $N_{1,y}$ were available, the value of $\varepsilon$ could conveniently be calculated via $\varepsilon = 4\left(\sigma_y/N_{1,y}\right)^2$.

### B. Uniaxial elongation

We next proceed to the case of uniaxial elongation. Figure 2 presents the dependency of $\lambda$ and the elongation stress as a function of dimensionless elongation rate, $\mathrm{Wi} = \dot{\varepsilon}\tau_{R,eq}$, for various values of $\varepsilon$ and $k$. We note, as for the shear flow, that as $\mathrm{Wi} \ll 1$, the elongation stress approaches its yield value $N_{\mathrm{E},y}$, given by Eq. (17b), whereas by increasing Wi, the network is destroyed [Fig. 2(a)] resulting in the increase of the elongation stress [Fig. 2(b)]. When, $k = 0$, the elongation stress diverges as Wi approaches ½, as is the prediction for the upper-convected Maxwell model.[41] However, when $k \neq 0$, the power-law behavior of the elongation stress at large Wi follows $N_{E,y} \sim \mathrm{Wi}^{-1/k}$. As in shear flow, $\varepsilon$ controls the behavior when $\mathrm{Wi} \ll 1$, whereas $k$ controls the behavior when $\mathrm{Wi} \gg 1$.

### C. Triangular change in shear rate experiments

We now turn our attention to the case of the time-dependent triangular change in the shear rate, which, as mentioned in Sec. I, is a characteristic rheological feature of thixotropic fluids. Here, the shear rate is initially increased as $\mathrm{Wi} = \mathrm{Wi}_{\max}(t/t_{\mathrm{m}})$, $0 < t < t_{\mathrm{m}}$, and then decreased following $\mathrm{Wi} = \mathrm{Wi}_{\max}[2 - (t/t_m)]$, $t_{\mathrm{m}} < t < 2t_{\mathrm{m}}$. The predictions for the shear stress and the first normal stress difference are plotted in Figs. 3 and 4, respectively. By increasing the absolute value of $k$, we note that the predictions for both quantities [Figs. 3(a) and 4(a)] decrease above $\mathrm{Wi} = 0.4$ in the ascending part of the shear-rate triangular ramp, but the overall shape of the

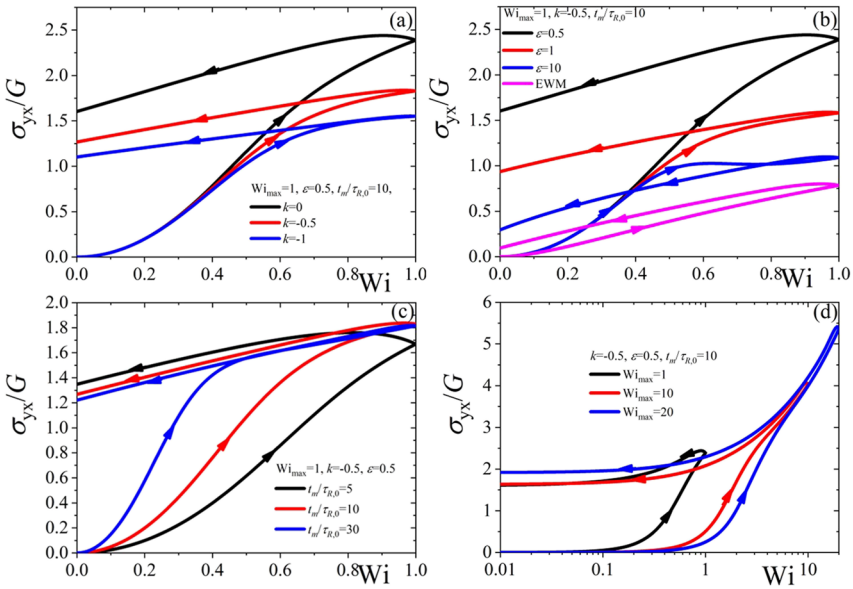


FIG. 3. Hysteresis curve predictions for the shear stress as a function of Wi for selected model parameter values.

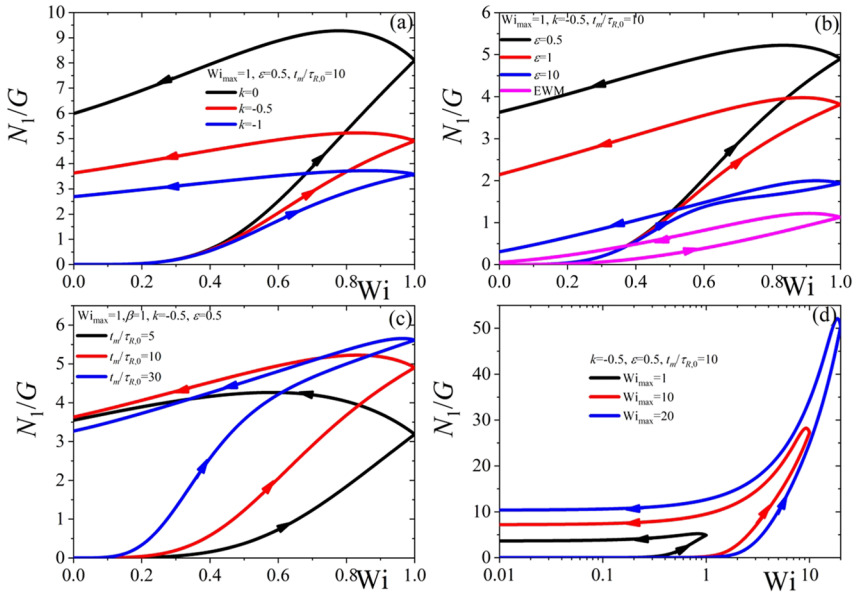


FIG. 4. Hysteresis curve predictions for the first normal stress difference as a function of Wi for selected model parameter values.

hysteresis loop remains the same, i.e., of the type depicted in Fig. 2(a) of Ref. 5; the same is noted when increasing the maximum shear rate [Figs. 3(d) and 4(d)], although, as expected, the predictions are higher as the shear rate becomes higher. Also, the same is noted by increasing $\varepsilon$; however, the overall shape of the curves is altered by having the two curves (the ascending and descending portions of the triangular ramp) coming closer to each other; in addition, the shear stress is seen to exhibit a large loop when $\varepsilon = 10$. Such a prediction is closer to the hysteresis curve type depicted in Fig. 2(c) of Ref. 5. Finally, by increasing the time needed to reach the maximum shear rate, $t_m$, the value of the stress and the first normal stress coefficient [Figs. 3(c) and 4(c)] increases, and the ascending and descending portions of the triangular ramp become more asymmetric and come closer to each other. As an overall note, the shear stress hysteresis loops are in a qualitative agreement with experimental rheological data for blood as measured by Bureau *et al.*[42] as will be made more clearly in Sec. VI.

## VI. COMPARISON WITH EXPERIMENTAL DATA

In Fig. 5, the model prediction is compared with the experimental steady-state shear data of Cloitre *et al.*[43] for the steady shear stress (scaled with the yield stress) as a function of dimensionless shear rate. The experimental data refer to soft colloidal pastes, consisting of polyelectrolyte microgels made of cross-linked acrylate chains bearing methacrylic acid units, of various concentrations in water ($\eta_s$ = 1 mPa s) or in a water/glycerol mixture ($\eta_s$ = 10 mPa s).[43] The characteristic time at equilibrium for non-associating segments is considered as $\tau_{R,eq} = \eta_s/G$ with $G = 4600(C\text{-}0.0142)$ given in Pa, and the value of $k = -3/4$ is selected to match the power-law at large shear rates, $\sigma_{yx} \sim \dot{\gamma}^{0.4}$. Figure 5 shows that the model is capable of reproducing the rheological data quite well except in the range $0.01 < \mathrm{Wi} < 1$. This could easily be amended by considering a spectrum of relaxation times instead of a single relaxation time as we have assumed here.

In Fig. 6, the model prediction is compared with the experimental steady-state shear stress data of Sousa *et al.*[44] on the whole blood of donor A, i.e., the solvent viscosity is about $\eta_s$ = 1.25 mPa s (the average value of the normal value of plasma viscosity is 1.16–1.33 mPa s at 37 °C independent of age and gender[45]). Given that at large shear rates $\sigma_{xy} \sim \dot{\gamma}$, then we consider $k = 0$. We note a very good comparison with the experimental rheological data, which were previously fitted with the Casson model.[46]

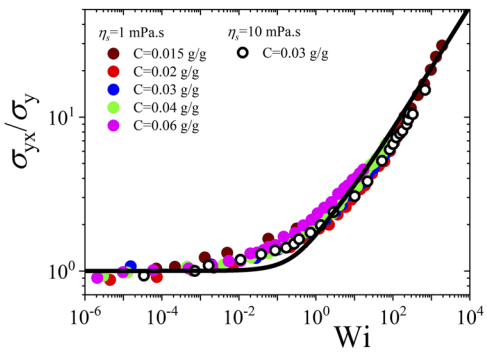


FIG. 5. Comparison of experimental rheological data of Cloitre *et al.*[43] on soft colloidal pastes (circles) along with the prediction (line) of the present model (with $\varepsilon = 1$ and $k = -3/4$ or $n = 0.4$).

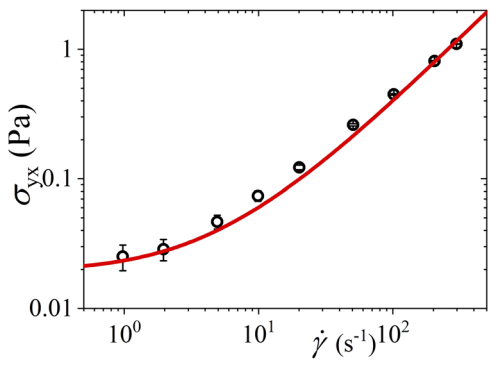


FIG. 6. Comparison of the model prediction (line) with the experimental rheological data (circles) on the blood of donor A from Ref. 44 with a hematocrit 41.6% at $T$ = 37 °C (with $G$ = 0.019 Pa, $\tau_{R,eq}$ = 0.14 s, $\varepsilon = 1$, and $k = 0$).

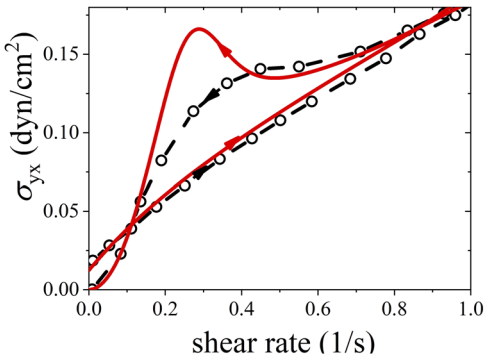


FIG. 7. Comparison of the prediction (continuous line) with the hysteresis curve-rheogram B data (circles connected with a dashed line) of sample 8 of Bureau *et al.*[42] (with $G = 0.28$ dyn/cm$^2$, $\tau_{R,eq} = 0.5$ s, $\varepsilon = 50$, and $k = 0$).

Finally, in Fig. 7, we compare the model prediction against the hysteresis curve-rheogram B of sample 8 ($\alpha = 0.043$ s$^{-2}$, $t_m = 23.8$ s) of Bureau *et al.*[42] (hematocrit equal to 45% and the measurements were done at 25 ± 0.5 °C). We consider a plasma viscosity equal to $\eta_s = 1.6$ mPa s[45] and consider blood to become Newtonian at large shear rates (i.e., $k = 0$). We note a satisfactory agreement with the experimental hysteresis curve of Bureau *et al.* although a slight mismatch is noted for the descending portion between, approximately, the shear rates 0.15 and 0.5.

## VII. CONCLUSION

We provided the modeling of materials exhibiting a thixotropic behavior through NET. Our approach provides the means to introduce a self-consistent coupling between elasticity and viscoplasticity. Even though the proposed model is simple, it has been shown to be able to capture the exhibition of a yield stress at small shear rates, and the power-law behavior at large shear rates in the case of steady shear, in accordance with rheological data routinely fitted with the HB model. It is important to say that the use of the Bingham and HB models in computational codes results in implementation difficulties due to the inherent singularity exhibited by the discontinuity of these models; i.e., they only flow above the yield stress.[8,47] The proposed model is free from such singularities. In addition, the proposed NET-based approach allows for checking the thermodynamic admissibility of the model. Moreover, it allows relating the notion of the yield stress to molecular arguments, which turns out to be governed by the ratio of the two characteristic times associated with the buildup of the network and the relaxation of segments. The new model is in quantitative agreement with steady-shear stress data of colloidal pastes (Fig. 5) and blood (Fig. 6), and in a satisfactory agreement with the rheological hysteresis data of blood as measured by Bureau *et al.*[42] (Fig. 7).

The proposed thermodynamically based approach, in addition to guaranteeing the thermodynamic admissibility and the internal consistency of the final transport equations, easily allows for important modifications, omitted in the present version of our model, to take place and thus improves its predictive capacity. The proposed model can be extended, for example, by considering an anisotropic hydrodynamic drag, which will allow the prediction of a non-vanishing second normal stress difference. Accounting for diffusion and wall effects will also be particularly important in reproducing the stress-gradient induced migration of red blood cells and rouleaux (column-like aggregates of red blood cells) to address the Fåhræus and Fåhræus–Lindqvist effects.[48] Such a modification would also be particularly important for drilling fluid flows in porous media.[49]

Finally, the improved constitutive model could be employed in direct finite element simulations which will improve our understanding as to how various parameters, such as temperature and pressure and the duration of stopping times in crude oil pipelines, affect the properties of crude oil.[9,50] Such results are expected to shed light on the rheological behavior of thixotropic materials and, therefore, to their tailor design. Given that thixotropic materials are used and consumed in everyday life, such an understanding is of great importance.

## ACKNOWLEDGMENTS

This work was partially co-funded by the Republic of Cyprus through the Research Promotion Foundation (Project No. KOYLTOYRA/BP-NE/0415/01) granted to P. S. Stephanou through the "Cyprus Research Award-Young Researcher 2015."

## APPENDIX: THERMODYNAMIC ADMISSIBILITY OF THE MODEL

Any thermodynamic system must obey the restriction of a non-negative total rate of entropy production. In the case of isothermal incompressible flows, the entropy production results from the degradation of mechanical energy leading to $dH_m/dt = [H_m, H_m] \leqslant 0$.[17] For this to be satisfied, for the model at hand, it can be shown that the following condition must hold:

$$-[H_m, H_m] = \int \left\{ \frac{\delta A}{\delta C_{\alpha\beta}} \Lambda^c_{\alpha\beta\gamma\varepsilon} \frac{\delta A}{\delta C_{\gamma\varepsilon}} + \Lambda^\lambda \left( \frac{\delta A}{\delta \lambda} \right)^2 + \nabla_\alpha \left( \frac{\delta H_m}{\delta M_\beta} \right) Q_{\alpha\beta\gamma\varepsilon} \nabla_\gamma \left( \frac{\delta H_m}{\delta M_\varepsilon} \right) \right\} dV \geq 0. \quad \text{(A1)}$$

The first term, written in terms of the dimensionless conformation tensor, gives

$$\frac{\delta A}{\delta \tilde{c}_{\alpha\beta}} \Lambda^c_{\alpha\beta\gamma\varepsilon} \frac{\delta A}{\delta \tilde{c}_{\gamma\varepsilon}} = \frac{G}{2\tau_R} \left( \mathrm{tr}\tilde{\mathbf{c}} - 6 + \mathrm{tr}\tilde{\mathbf{c}}^{-1} \right), \quad \text{(A2a)}$$

or when rewritten in terms of the eigenvalues of the conformation tensor, $\mu_k \{k = x, y, z\}$,

$$\frac{\delta A}{\delta \tilde{c}_{\alpha\beta}} \Lambda^c_{\alpha\beta\gamma\varepsilon} \frac{\delta A}{\delta \tilde{c}_{\gamma\varepsilon}} = \frac{G}{2\tau_R} \sum_k \frac{(\mu_k - 1)^2}{\mu_k} \geq 0. \quad \text{(A2b)}$$

Given that both the characteristic time and the elastic modulus are always positive, this is indeed a non-negative quantity. The second term in Eq. (A1) is non-negative provided that $\Lambda^\lambda \geq 0$ which, in view of Eq. (10b), indeed holds true for a non-negative relaxation time $\tau_\lambda$. Finally,

$$\nabla_\alpha\left(\frac{\delta H_m}{\delta M_\beta}\right)Q_{\alpha\beta\gamma\varepsilon}\nabla_\gamma\left(\frac{\delta H_m}{\delta M_\varepsilon}\right) = \eta_s\dot{\boldsymbol{\gamma}}:\dot{\boldsymbol{\gamma}} \geq 0, \qquad \text{(A2c)}$$

which holds true for a non-negative solvent viscosity.

In the above description, it has been assumed that the conformation tensor is positive definite. A sufficient (but not necessary) condition for the conformation tensor to be positive definite is the prefactor of the unit tensor in the conformation tensor evolution equation [Eq. (11)] be non-negative;[17,51] this requires that $\tau_R \geq 0$, which holds true since characteristic times are always non-negative. Thus, it has been demonstrated that the derived model is thermodynamically admissible and preserves the positive-definite nature of the conformation tensor.


[1] P. Coussot, "Yield stress fluid flows: A review of experimental data," J. Non-Newtonian Fluid Mech. **211**, 31 (2014).
[2] P. Coussot, "Slow flow of yield-stress fluids: Yielding liquids or flowing solids," Rheol. Acta **57**, 1–14 (2018).
[3] P. Coussot, "Bingham's heritage," Rheol. Acta **56**, 163 (2017).
[4] N. J. Balmforth, I. A. Frigaard, and G. Ovarlez, "Yielding to stress: Recent developments in viscoplastic fluid mechanics," Annu. Rev. Fluid. Mech. **46**, 121 (2014).
[5] J. Mewis and N. J. Wagner, "Thixotropy," Adv. Colloid Interface Sci. **147-148**, 214 (2009).
[6] IUPAC, Compendium of Chemical Terminology, electronic version, http://goldbook.iupac.org.W06691.html.
[7] R. G. Larson, "Constitutive equations for thixotropic fluids," J. Rheol. **59**, 595–611 (2015).
[8] E. Mitsoulis, "Flows of viscoplastic materials: Models and computations," Rheol. Rev. **2007**, 135–178.
[9] S. Livescu, "Mathematical modeling of thixotropic drilling mud and crude oil flow in wells and pipelines—A review," J. Pet. Sci. Eng. **98-99**, 174 (2012).
[10] A. M. V. Putz and T. I. Burghelea, "The solid–fluid transition in a yield stress shear thinning physical gel," Rheol. Acta **48**, 673 (2009).
[11] A. N. Alexandrou, N. Constantinou, and G. Georgiou, "Shear rejuvenation, aging and shear banding in yield stress fluids," J. Non-Newtonian Fluid Mech. **158**, 6 (2009).
[12] F. Moore, "The rheology of ceramic slips and bodies," Trans. Br. Ceram. Soc. **58**, 470–494 (1959).
[13] A. G. Fredrickson, "A model for the thixotropy of suspensions," AIChE J. **16**, 436–441 (1970).
[14] P. Saramito, "A new constitutive equation for elastoviscoplastic fluid flows," J. Non-Newtonian Fluid Mech. **145**, 1 (2007); "A new elastoviscoplastic model based on the Herschel–Bulkley viscoplastic model," **158**, 154 (2009).
[15] Y. S. Park and P. L. F. Liu, "Oscillatory pipe flows of a yield-stress fluid," J. Fluid Mech. **658**, 211 (2010).
[16] D. Fraggedakis, Y. Dimakopoulos, and J. Tsamopoulos, "Yielding the yield stress analysis: A thorough comparison of recently proposed elasto-visco-plastic (EVP) fluid models," J. Non-Newtonian Fluid Mech. **238**, 170 (2016).
[17] A. N. Beris and B. J. Edwards, *Thermodynamics of Flowing Systems with Internal Microstructure* (Oxford University Press, London, 1994).
[18] M. Grmela and H. C. Öttinger, "Dynamics and thermodynamics of complex fluids. I. Development of a general formalism," Phys. Rev. E **56**, 6620 (1997); H. C. Öttinger and M. Grmela, "Dynamics and thermodynamics of complex fluids. II. Illustrations of a general formalism," *ibid.* **56**, 6633 (1997).
[19] H. C. Öttinger, *Beyond Equilibrium Thermodynamics* (Wiley, Hoboken, NJ, USA, 2005).
[20] B. J. Edwards, A. N. Beris, and M. Grmela, "Generalized constitutive equation for polymeric liquid crystals: Part 1. Model formulation using the Hamiltonian (Poisson bracket) formulation," J. Non-Newtonian Fluid Mech. **35**, 51–72 (1990).
[21] B. J. Edwards, A. N. Beris, M. Grmela, and R. G. Larson, "Generalized constitutive equation for polymeric liquid crystals: Part 2. Non-homogeneous systems," J. Non-Newtonian Fluid Mech. **36**, 243–254 (1990).
[22] B. J. Edwards, "The dynamical continuum theory of liquid crystals," Ph.D. thesis, University of Delaware, 1991.
[23] P. S. Stephanou, C. Baig, and V. G. Mavrantzas, "A generalized differential constitutive equation for polymer melts based on principles of nonequilibrium thermodynamics," J. Rheol. **53**, 309 (2009).
[24] P. S. Stephanou, I. Ch. Tsimouri, and V. G. Mavrantzas, "Flow-induced orientation and stretching of entangled polymers in the framework of nonequilibrium thermodynamics," Macromolecules **49**, 3161 (2016).
[25] A. N. Beris and B. J. Edwards, "Poisson bracket formulation of viscoelastic flow equations of differential type: A unified approach," J. Rheol. **34**, 503–538 (1990).
[26] M. Dressler and B. J. Edwards, "The influence of matrix viscoelasticity on the rheology of polymer blends," Rheol. Acta **43**, 257 (2004).
[27] M. Dressler and B. J. Edwards, "Rheology of polymer blends with matrix-phase viscoelasticity and a narrow droplet size distribution," J. Non-Newtonian Fluid Mech. **120**, 189 (2004).
[28] M. Dressler, B. J. Edwards, and E. J. Windhab, "An examination of droplet deformation and break-up between concentrically rotating cylinders," J. Non-Newtonian Fluid Mech. **152**, 86 (2008).
[29] M. Rajabian, C. Dubois, and M. Grmela, "Suspensions of semiflexible fibers in polymeric fluids: Rheology and thermodynamics," Rheol. Acta **44**, 521 (2005).
[30] H. Eslami, M. Grmela, and M. Bousmina, "A mesoscopic rheological model of polymer/layered silicate nanocomposites," J. Rheol. **51**, 1189 (2007).
[31] H. Eslami, M. Grmela, and M. Bousmina, "A mesoscopic tube model of polymer/layered silicate nanocomposites," Rheol. Acta **48**, 317 (2009).
[32] M. Rajabian, G. Naderi, P. J. Carreau, and C. Dubois, "Flow-induced particle orientation and rheological properties of suspensions of organoclays in thermoplastic resins" J. Polym. Sci., Part B: Polym. Phys. **48**, 2003 (2010).
[33] P. S. Stephanou, V. G. Mavrantzas, and G. C. Georgiou, "Continuum model for the phase behavior, microstructure, and rheology of unentangled polymer nanocomposite melts," Macromolecules **47**, 4493 (2014).
[34] P. S. Stephanou, "How the flow affects the phase behaviour and microstructure of polymer nanocomposites," J. Chem. Phys. **142**, 064901 (2015).
[35] P. S. Stephanou, "The rheology of drilling fluids from a non-equilibrium thermodynamics perspective," J. Pet. Sci. Eng. **165**, 1010 (2018).
[36] I. Ch. Tsimouri, P. S. Stephanou, and V. G. Mavrantzas, "A constitutive rheological model for agglomerating blood derived from nonequilibrium thermodynamics," Phys. Fluids **30**, 030710 (2018).
[37] M. Kumar, B. J. Edwards, and S. J. Paddison, "A macroscopic model of proton transport through the membrane-ionomer interface of a polymer electrolyte membrane fuel cell," J. Chem. Phys. **138**, 064903 (2013).
[38] A. N. Beris, E. Stiakakis, and D. Vlassopoulos, "A thermodynamically consistent model for the thixotropic behavior of concentrated star polymer suspensions," J. Non-Newtonian Fluid Mech. **152**, 76 (2008).
[39] A. Souvaliotis and A. N. Beris, "An extended White–Metzner viscoelastic fluid model based on an internal structural parameter," J. Rheol. **36**, 241 (1992).
[40] M. Rubinstein and R. H. Colby, *Polymer Physics*, 1st ed. (Oxford University Press, 2003).
[41] R. B. Bird, C. F. Curtiss, R. C. Armstrong, and O. Hassager, *Dynamics of Polymeric Liquids: Vol. 2, Kinetic Theory*, 2nd ed. (John Wiley & Sons, New York, 1987).
[42] M. Bureau, J. C. Healy, D. Bourgoin, and M. Joly, "Rheological hysteresis of blood at low shear rate," Biorheology **17**, 191 (1980).
[43] M. Cloitre, R. Borrega, F. Monti, and L. Leibler, "Glassy dynamics and flow properties of soft colloidal pastes," Phys. Rev. Lett. **90**, 068303 (2003).
[44] P. C. Sousa, J. Carneiro, R. Vaz, A. Cerejo, F. T. Pinho, M. A. Alves, and M. S. N. Oliveira, "Shear viscosity and nonlinear behavior of whole blood under large amplitude oscillatory shear," Biorheology **50**, 269–282 (2013).
[45] International Committee for Standardization in Haematology, "Recommendation for a selected method for the measurement of plasma viscosity," J. Clin. Pathol. **37**, 1147–1152 (1984).
[46] A. J. Apostolidis, M. J. Armstrong, and A. N. Beris, "Modeling of human blood rheology in transient shear flows," J. Rheol. **59**, 275 (2015).
[47] E. Mitsoulis and J. Tsamopoulos, "Numerical simulations of complex yield-stress fluid flows," Rheol. Acta **56**, 231 (2017).

[48]T. W. Secomb and A. R. Pries, "Blood viscosity in microvessels: Experiment and theory," C. R. Phys. **14**, 470 (2013).
[49]R. Majidi, S. Z. Miska, M. Yu, L. G. Thompson, and J. Zhang, "Modeling of drilling fluids in naturally fractured formations," in *SPE Annual Technical Conference and Exhibition, 21–24 September 2008* (SPE, Denver, Colorado, USA, 2008), p. 114630.
[50]G. T. Chala, S. A. Sulaiman, and A. Japper-Jaafar, "Flow start-up and transportation of waxy crude oil in pipelines—A review," J. Non-Newtonian Fluid Mech. **251**, 69 (2018).
[51]M. A. Hulsen, "A sufficient condition for a positive definite configuration tensor in differential models," J. Non-Newtonian Fluid Mech. **38**, 93 (1990).